
Resilient Voltage Estimation for Battery Packs Using Self-Learning Koopman Operator

A PREPRINT

Sanchita Ghosh¹ and Tanushree Roy¹

¹Department of Mechanical Engineering, Texas Tech University, Lubbock, TX 79409, US.
Emails: sancghos@ttu.edu, tanushree.roy@ttu.edu.

February 12, 2026

ABSTRACT

Cloud-based battery management systems (BMSs) rely on real-time voltage measurement data to ensure coordinated bi-directional charging of electric vehicles (EVs) with vehicle-to-grid technology. Unfortunately, an adversary can corrupt the measurement data during transmission from the local-BMS to the cloud-BMS, leading to disrupted EV charging. Therefore, to ensure reliable voltage data under such sensor attacks, this paper proposes a two-stage error-corrected self-learning Koopman operator-based secure voltage estimation scheme for large-format battery packs. The first stage of correction compensates for the Koopman approximation error. The second stage aims to recover the error amassing from the lack of higher-order battery dynamics information in the self-learning feedback, using two alternative methods: an adaptable empirical strategy that uses cell-level knowledge of open circuit voltage to state-of-charge mapping for pack-level estimation, and a Gaussian process regression-based data-driven method that leverages minimal data-training. During our comprehensive case studies using the high-fidelity battery simulation package ‘PyBaMM-liionpack’, our proposed secure estimator reliably generated real-time voltage estimation with high accuracy under varying pack topologies, charging settings, battery age-levels, and attack policies. Thus, the scalable and adaptable algorithm can be easily employed to diverse battery configurations and operating conditions, without requiring significant modifications, excessive data or sensor redundancy, to ensure optimum charging of EVs under compromised sensing.

1 Introduction

The transition towards cleaner and more environmental-friendly energy operations, combined with sustainability mandates, has motivated the widespread adoption of renewable energy systems in modern power grids [1]. Additionally, with rapid advancements in Lithium-ion batteries and vehicular electrification, the electric vehicle (EV) infrastructure has emerged as the preferred choice for ancillary power services, including energy storage to support this transition toward sustainable energy [2]. Large-scale deployment of EV infrastructure coordinated with renewable energy systems can contribute to (i) reduced energy price, (ii) less reliance on fossil-fuel resources, (iii) lower carbon footprint, (iv) less emission of greenhouse gases, and (v) improved grid stability with reduced voltage fluctuation, and (vi) enhanced power quality [3]. Nevertheless, such growing integration of EV infrastructure in smart grids also introduces challenges in ensuring optimum battery operations and grid stability with reduced energy cost, while safeguarding the battery health [4]. Therefore, battery management systems (BMSs) play a critical role in enhancing the efficiency, safety, and lifespan of these batteries by real-time monitoring and regulation of key battery states such as state of charge, temperature, or voltage [5]. Additionally, BMSs often operate in a cyber-physical environment to accommodate large-scale deployment of these batteries, i.e., the BMS is implemented in the cloud environment to leverage high computational resources and coordinability across distributed networks [6]. Unfortunately, such cyber-physical BMS operations exhibit inherent security risks that can result in financial and energy losses, grid instability, or even unsafe battery operations [7]. This necessitates the research on cybersecurity analysis for BMS to

ensure safe EV charging as well as reliable grid operations against cyberattacks [8, 9].

To address the security challenges in BMS and EV charging infrastructure, researchers investigated the vulnerabilities of the EV charging infrastructure and their plausible disruptive impact on power grid operations [10]. Moreover, researchers showed that the vulnerabilities in EVs and EV charging stations can be exploited to induce widespread grid disturbances, power outages, over-frequency, and low power factor [11, 12]. Similarly, [8] provided a comprehensive threat assessment to identify the adversarial impact on functionality, safety, and performance of BMS due to several cyberattacks and illustrated how compromised sensing can mislead BMS to making unsafe decisions, resulting in erroneous control actions and poor battery management. Accordingly, authors proposed an extended Kalman filter-based algorithm to detect false-data-injection (FDI) sensor attacks in battery stacks in [13]. Similarly, machine learning models such as convolutional neural networks [14], long short-Term memory networks [15], and supervised classifiers [16] have been adopted to develop cyberattack detection algorithms for EV charging infrastructure. In [17], authors utilized the principal component analysis-based unsupervised k-means strategy to detect the presence of cell-voltage buffer manipulation cyberattacks in BMS. Moreover, the authors proposed a Koopman operator-based algorithm to detect both actuation and sensor attacks and, thereafter, isolate the source of the attack in [18].

Upon reliable detection of these cyberattacks, it is crucial to develop countermeasure strategies to promptly mitigate the impact of cyberattacks while evading safety-critical threats and widespread grid disturbances [19, 20]. In particular, sensor attacks are designed to deceive the cloud-BMS and administrators about the true operating conditions of the system, and in general, remain harder to mitigate without sensor redundancy [21]. Moreover, failure to mitigate sensor attacks can lead to incorrect control actions, poor battery management, reduced battery life, and unpredictable failures such as thermal runaway, fires, or explosions [8]. Consequently, in [22], authors proposed an equivalent-circuit model (ECM)-based non-linear estimator for Li-ion batteries to ensure secure state-of-charge (SOC) estimation under compromised sensing, while identifying the ECM parameters with an extended Kalman filter. In [19], authors utilized a time-varying recursive Kalman filter to generate secure SOC estimation under low-intensity deception attacks upon detection. Similarly, [23] proposed a sensor attack detection and compensation scheme for EV battery systems and leveraged the discrepancy between set-membership of the state estimation and prediction to estimate the battery SOC under sensor attacks. Moreover, [24] adopted an impulsive-driven-based observer to estimate SOC that acquires measurement data at discrete instants rather than using a continuous data stream to reduce susceptibility to attacks as well as to minimize the cumulative impact of compromised data on estimation, and shows that the observer achieves improved estimation accuracy under compromised sensing.

While these studies highlight the crucial need for resilient sensing in batteries under sensor attacks, they also reveal several key research gaps. These works adopt a model-based approach for secure estimation and thus face challenges from the scarcity of reliable Li-ion battery models [25]. Additionally, model-based algorithms, in general, exhibit high computational complexities and poor scalability to varied pack configuration [21]. Moreover, the estimation method must not rely on rigid assumptions regarding cyberattacks or prior attack knowledge. Although our previous paper [26] presents the proof of concept of a self-learning feedback mechanism for Koopman operator-based secure estimation in battery systems, the proposed algorithm is validated using only a single-cell Li-ion battery with fixed parameter ECM. Hence, [26] fails to address the lack of scalable algorithms in the existing literature. Furthermore, [26] did not consider realistic internal dynamics of the battery and utilized an arbitrary sampling frequency for voltage measurement. Thus, our preliminary work [26] motivates the research scope for further explorations to substantiate the applicability of our secure estimation algorithm in real-world scenarios. Our contribution addresses these gaps in the following way:

1. We proposed an error compensated self-learning Koopman operator-based secure voltage estimation for large-format battery packs under sensor cyberattacks. The error compensation of the self-learning feedback is implemented in two stages to eliminate the errors amassing from the Koopman approximation and the lack of higher-order dynamics data from the battery. The proposed data-driven secure estimator adopts a small-data online learning approach that requires only limited model information and does not rely on sensor redundancy.
2. For the error correction, we propose an interpretable and scalable battery characteristic-guided heuristic correction for the self-learning Koopman operator that readily utilizes cell-level knowledge for pack-level estimation without any added computational burden.
3. Alternatively, we also propose a GPR-based data-driven error compensation strategy that requires minimal offline data for training and eliminates the need for battery characteristic information.
4. We validate our error compensated self-learning Koopman-based secure estimator using rate-limited, online battery voltage measurements and charging current data that are generated from a high-fidelity simulation

package ‘PyBaMM-liionpack’ [27], while considering varied pack topologies, charging settings, battery age-levels, and cyberattack scenarios to demonstrate the feasibility of our method in practical deployment.

The rest of the paper is organized as follows. Section 2 presents the problem framework of this paper. Next, we introduce our proposed self-learning Koopman-based secure estimation algorithm along with two-staged error compensation strategies. Our simulation results are presented in Section 4. Finally, Section 5 concludes our paper.

2 Problem Formulation

This paper addresses the problem of secure voltage estimation during EV charging operation in the presence of sensor cyberattacks. In this section, we first describe the EV charging infrastructure with the corresponding cyberattack policies. Next, we present a brief overview of Koopman linear battery model, followed by the event-triggering mechanism under sensor attacks.

2.1 Electric Vehicle Charging Under Compromised Sensing

In this paper, we consider that a cloud-based BMS monitors the voltage measurements of the EV from the local-BMS as well as the grid data to provide the appropriate charging or discharging current actuation command to the local-BMS to support bi-directional energy exchange with V2G application. Both the voltage measurements from the local-BMS to the cloud-BMS and the actuation command from the cloud-BMS to the local-BMS are sent through communication channels that are susceptible to cyberattacks [18]. Measurement corruption is known as sensor attack, while input signal corruption is known as actuation attack [28]. In this framework, we consider that an adversary injects a sensor attack δ to corrupt the voltage measurements, and the battery charging dynamics in this scenario is defined as follows:

$$x(k+1) = f(x(k), I_c(k)); \quad V(k) = g(x(k)) + \delta(k). \quad (1)$$

Here, $x(k) \in \mathbb{X} \subset \mathbb{R}^d$ represents the internal battery states at k^{th} instant that may include lithium-ion concentrations, solid and liquid phase potentials, open circuit potential, etc. [29]. $V(k) \in \mathbb{R}^m$ is the module voltage measurements at the k^{th} instant as $V(k) = [V_1(k) \quad \dots \quad V_m(k)]^T$ and m is the total number of modules in the pack. $\delta(k)$ is the sensor cyberattack that corrupts the voltage measurements at k^{th} instant. $I_c \in \mathbb{U} \subset \mathbb{R}$ is the input current signal such that the positive value of I_c indicates discharging, and the negative value indicates charging. The non-linear function $f : \mathbb{X} \times \mathbb{U} \rightarrow \mathbb{X}$ captures the internal dynamics of the battery and $g : \mathbb{X} \rightarrow \mathbb{R}^m$ defines the non-linear measurement function.

Sensor attacks on bi-directional charging of EV pose a severe and critical risk, since inaccurate voltage measurements can lead to poor battery management and undesired or even unsafe battery operations. Moreover, such sensor attacks can initiate erroneous control actions from the cloud-BMS that can result in widespread disturbances in the grid. While actuation attacks can cause severe outcomes with direct impact on the system, their impact can be detected more readily and mitigated through safety constraints or actuation removal. However, it is difficult to assess the impact of the sensor attacks in real-time due to the unavailability of perfect measurement knowledge, and in general remain harder to mitigate without sensor redundancy. Thus, secure estimation under compromised sensing is crucial to ensure reliable control of EV charging.

Therefore, we propose an event-triggered secure estimator for the EV battery subjected to a sensor attack. A Koopman-based diagnostic algorithm (proposed in our previous paper [18]) is utilized to activate the secure voltage estimation upon the identification of a sensor attack. We adopt a self-learning Koopman approach for the secure estimator that runs with error-compensated self-feedback to obtain the reliable estimation \hat{V} for the module voltage data V , when $\delta \neq 0$. Finally, cloud-BMS utilizes the secure module voltage estimation \hat{V} to ensure safe and optimum bi-directional charging of EVs. Fig. 1 captures the overview of our problem framework.

Next, we outline the realization of the Koopman operator (KO) regarding the battery dynamics (1).

2.2 Koopman Linear Model for Battery

We utilize KO theory combined with advanced data-driven techniques to obtain a transformation $x \mapsto z$ such that the *nonlinear* battery dynamics in x can be embedded in a *linear* state dynamics in z [30]. To define the KO for the battery system (1), let us first define $l(\mathbb{U})$ as the space of all possible input current sequences $\mathbf{I}_c = \{I_c(k)\}_{k=0}^{\infty}$ with $I_c(k) \in \mathbb{U}$ and a right shift operator $\mathbf{S} : l(\mathbb{U}) \rightarrow l(\mathbb{U})$, i.e., $\mathbf{S}\mathbf{I}_c(k) = \mathbf{I}_c(k+1), \forall k$ and $\mathbf{I}_c(k)$ is the k^{th} element of \mathbf{I}_c . Now, we consider an infinite-dimensional Hilbert space \mathcal{H} such that $\psi \in \mathcal{H}$ is a complex-valued observable

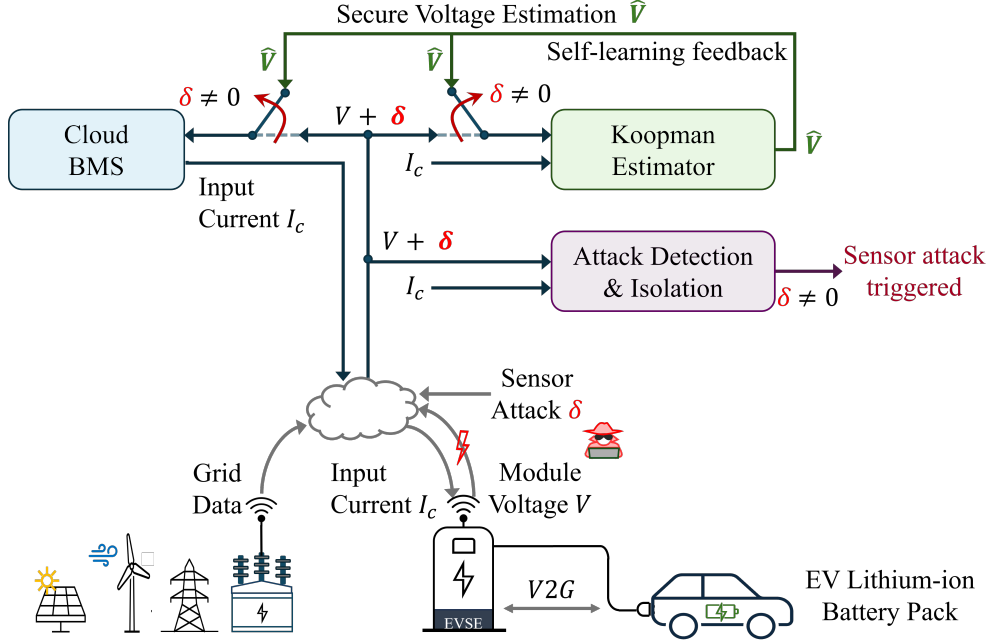


Figure 1: Block diagram shows the secure voltage estimation generation under sensor attack.

function and $\psi : \mathbb{X} \times l(\mathbb{U}) \rightarrow \mathbb{C}$. Then for any observable function ψ , state x , and input I_c , the set of KO on this space, $\mathcal{K} : \mathcal{H} \rightarrow \mathcal{H}$ is defined as

$$\begin{aligned} (\mathcal{K}\psi)(x(k), \mathbf{I}_c(k)) &= \psi(f(x(k), I_c(k)), \mathbf{SI}_c(k)) \\ &= \psi(x(k+1), \mathbf{I}_c(k+1)). \end{aligned} \quad (2)$$

Additionally, there exist infinitely many eigen-observable functions, $\phi_i : \mathbb{X} \times l(\mathbb{U}) \rightarrow \mathbb{C}$, that span the observable space \mathcal{H} as $\mathcal{H} = \text{span}\{\phi_i\}_{i=1}^{\infty}$, and the KO \mathcal{K} evolves these eigenfunctions ϕ linearly in time with the corresponding Koopman eigenvalues, $\lambda \in \mathbb{C}$ as [31, 32]:

$$\begin{aligned} \phi(x(k+1), \mathbf{I}_c(k+1)) &= \mathcal{K}\phi(x(k), \mathbf{I}_c(k)) \\ &= \lambda\phi(x(k), \mathbf{I}_c(k)). \end{aligned} \quad (3)$$

Then $\psi(x(k), \mathbf{I}_c(k))$ can be expanded in terms of ϕ s and λ s as $\psi(x(k), \mathbf{I}_c(k)) = \sum_{i=1}^{\infty} \lambda_i^k \phi_i(x(0), \mathbf{I}_c(0)) v_i^{\psi}$. Here the Koopman Modes (KM) $v_i^{\psi} \in \mathbb{C}^{\psi}$ are the coefficients of the projection of $\psi(x)$ onto the $\text{span}\{\phi_i\}_{i=1}^{\infty}$ [33]. Moreover, the measurement function g in (1) can similarly be expanded in ϕ s with corresponding KMs $v_i^g \in \mathbb{C}^n$ [34].

Next, we adopt delay embedding along with dynamic mode decomposition (DMD) techniques to address the infinite dimensionality of the KO during practical implementation. In particular, we utilize these techniques to obtain a finite set of ϕ s to span a Koopman invariant subspace such that the ϕ s remain in that subspace after the Koopman operation [31]. Furthermore, if the measurement function g lies in the subspace spanned by the finite set of ϕ s, a good approximation can be achieved by

$$g(x(k)) = \sum_{i=1}^n \phi_i(x(k), \mathbf{I}_c(k)) v_i^g. \quad (4)$$

Remark 1. It should be noted from (3) and (4) that the Koopman eigenfunctions and eigenvalues solely depend on the system dynamics f and the function space \mathcal{H} . On the other hand, the KMs are specific to the corresponding observable, e.g., v_i^g depends on the measurement function g . Consequently, during an actuation attack only the ϕ s and λ s are affected explicitly, contrarily a sensor attack impacts the KMs v_i^g .

To implement this method, while ensuring small data learning and computational efficiency, the KO is learned online over a sliding window of battery data. During each sliding window, we utilize the available data to learn the Koopman

linear model, and this learned model is utilized to generate module voltage predictions V_p over a receding horizon. Hence, we consider a sliding window sequence of S observations and divide it into two data sub-sequences, namely learning window \mathfrak{L} with length $\tilde{S} < S$ and prediction window \mathfrak{P} with length $S - \tilde{S}$ as:

$$\mathfrak{L} \in \{k + 1, \dots, k + \tilde{S}\}, \mathfrak{P} \in \{k + \tilde{S} + 1, \dots, k + S\}. \quad (5)$$

Here, the sliding window moves forward with $S - \tilde{S}$ amount after every prediction cycle. During each learning window, we utilize the limited available voltage measurement and input charging current data stack ζ_V and ζ_U (6)-(7) to approximate the KO for the battery system.

$$\zeta_V = [V^T(k+1) \ \dots \ V^T(k+\tilde{S})], \quad (6)$$

$$\zeta_U = [U^T(k+1) \ \dots \ U^T(k+\tilde{S})]. \quad (7)$$

Now, we rearrange these data to embed delay as follows.

$$\xi = [D_{k+1} \ D_{k+2} \ \dots \ D_{k+\tilde{S}-\tau-1}], \quad (8)$$

$$\xi^+ = [D_{k+2} \ D_{k+3} \ \dots \ D_{k+\tilde{S}-\tau}], \quad (9)$$

$$U = [I_c(k+1+\tau) \ \dots \ I_c(k+\tilde{S}-1)], \quad (10)$$

$$\text{where, } D_k = [V^T(k) \ I_c(k) \ \dots \ V^T(k+\tau)]^T. \quad (11)$$

Here, τ is the embedded delay. Next, adopting the DMD technique and using these delay embedded battery data matrices, we obtain the approximate Koopman linear model as follows:

$$z(k+1) = A_{\mathfrak{L}} z(k) + B_{\mathfrak{L}} I_c(k); \quad V_p(k) \approx C_{\mathfrak{L}} z(k). \quad (12)$$

Here, (12) is the Koopman linear model for the battery system (1), approximated from the limited available battery data and $V_p(k)$ is the predicted module voltage measurements at the k -th time instant. The matrices $A_{\mathfrak{L}}$, $B_{\mathfrak{L}}$, and $C_{\mathfrak{L}}$ are re-learned at each sliding window. $A_{\mathfrak{L}} \in \mathbb{R}^{n \times n}$ and $B_{\mathfrak{L}} \in \mathbb{R}^{n \times 1}$ contain the Koopman eigenvalues. Moreover, the transformed state $z \in \mathbb{R}^n$ and the output matrix $C_{\mathfrak{L}} \in \mathbb{R}^{m \times n}$ are given by,

$$z = [\hat{\phi}_1(x, \mathbf{I}_c) \ \dots \ \hat{\phi}_n(x, \mathbf{I}_c)]^T, \quad C_{\mathfrak{L}} = [\hat{v}_1^g \ \dots \ \hat{v}_n^g]. \quad (13)$$

Here, real-valued $\hat{\phi}_i$ and \hat{v}_i^g are generated, respectively, from complex-valued ϕ_i and v_i^g in the following manner. If $\phi_i(x)$ is real, then $\hat{\phi}_i = \phi_i$ and $\hat{v}_i^g = v_i^g$. Whereas, if $\phi_i(x)$ and ϕ_{i+1} are complex-conjugate pairs, then $[\hat{\phi}_i \ \hat{\phi}_{i+1}] = [2\text{Re}(\phi_i) \ -2\text{Im}(\phi_i)]$ and $[\hat{v}_i^h \ \hat{v}_{i+1}^h] = [\text{Re}(v_i^h) \ \text{Im}(v_i^h)]$ [35]. This finite approximation of the associated KO (i.e., corresponding $A_{\mathfrak{L}}$, $B_{\mathfrak{L}}$, and $C_{\mathfrak{L}}$) can be estimated from the optimization problems posed below.

$$\text{Opt 1 : } \min_{\Lambda} \|\xi^+ - \Lambda \Xi\|_F, \quad \text{Opt 2 : } \min_{C_{\mathfrak{L}}} \|Y - C_{\mathfrak{L}} \xi\|_F, \quad (14)$$

where, $\Lambda = [A_{\mathfrak{L}} \ B_{\mathfrak{L}}]$, $\Xi = [\zeta^T \ U^T]^T$, and $Y = [V^T(k+1) \ \dots \ V^T(k+\tilde{S}-\tau-1)]$. Here, $\|(\cdot)\|_F$ denotes the Frobenius norm of a matrix. The analytical least-square solutions of $O1$ and $O2$ in (14) can be found using pseudo-inverse such as $\Lambda = \xi^+ \Xi^\dagger$ and $C_{\mathfrak{L}} = Y \xi^\dagger$, respectively.

2.3 Identification of Sensor Attacks

We utilize a KO-based diagnostic (KOD) algorithm to reliably identify the presence of sensor attacks and activate the secure estimator. The KOD algorithm utilizes (14) to learn the Koopman linear model at each learning window and evolves the learned model as (12) to generate module voltage predictions V_p for the following prediction window. The algorithm monitors the detection residual $RD = V - V_p$, i.e., the difference between the true and predicted voltage data to capture the presence of an attack, and an attack decision is made when the residual RD crosses a predefined threshold. Next, the KOD algorithm utilizes the Remark 1 to capture the distinct signatures of actuation and sensor attacks on Koopman eigenfunctions ϕ_i and modes v_i^g , respectively. In particular, the algorithm monitors the deviation in KMs v_i^g due to the presence of an attack as the isolation residual RI , and a sensor attack is identified if the residual RI crosses a predefined threshold (vide reference [18] for details of the KOD algorithm). Once the presence of a sensor attack is identified, we activate the proposed secure estimator.

3 Secure Terminal Voltage Estimation Algorithm

In this section, we present our proposed error compensation-integrated self-learning KO-based secure estimation algorithm. This estimation method has two parts: (A) Koopman-based voltage prediction using self-learning feedback and (B) two-staged corrections of prediction error. We also propose two alternative methods for the second-stage error correction: (i) an interpretable empirical strategy based on open circuit voltage (OCV) to SOC mapping and (ii) a training-efficient data-driven method based on the Gaussian process regression technique.

3.1 Koopman-based prediction with self-learning feedback

To generate module voltage predictions online, we deploy (12)-(14) to effectively learn the Koopman linear model from limited available data (8)-(11), when $\delta = 0$. However, when the KOD algorithm identifies a sensor attack and triggers the secure estimation algorithm ($\delta \neq 0$), corrupted module voltage measurements are excluded from updating the Koopman operator. Instead, the secure estimator starts to utilize the Koopman prediction V_p as feedback to itself, i.e., it initiates self-learning feedback.

Consequently, after some time, the secure estimator uses a data stack consisting of only voltage predictions. Thus, under nominal EV charging ($\delta = 0$), the Koopman voltage predictor runs with measurement feedback from the data stack ζ_V in (6). Conversely, in the presence of a sensor attack ($\delta \neq 0$), the Koopman voltage predictor is approximated using the self-learning feedback from the data stack ζ_{V_p} in (15) such that the corrupted voltage measurement data V are replaced with the Koopman predictions V_p .

$$\zeta_{V_p} = [V_p^T(k+1) \ \cdots \ V_p^T(k+\tilde{S})]. \quad (15)$$

In contrast, for both nominal and secure estimation operations, the Koopman predictor utilizes the input data stack ζ_U in (7). Consequently, under compromised sensing ($\delta \neq 0$), the self-learning Koopman-based voltage predictor utilizes the data matrices ζ_{V_p} and ζ_U , respectively, in (15) and (7) to learn Koopman linear model (12), and thus, mitigate the adversarial impact of the sensor attack δ .

Nevertheless, such simplified self-learning KO introduces two drawbacks. Firstly, if the secure estimator receives only V_p for self-learning feedback, it will accumulate prediction errors from the Koopman linear approximation. Next, the self-learning Koopman predictor will cease to capture any higher-order changes in the battery dynamics due to the lack of new system information in the self-learning feedback and this leads to further error accumulation. Hence, we propose two-stage error corrections for the V_p feedback to address these inaccuracies due to the Koopman approximation (stage I) and the higher-order battery dynamics (stage II).

3.2 Stage I: Koopman approximation error correction

During this stage of error correction, we consider compensating for the potential prediction error due to the Koopman linear approximation in (14). Let us first denote V_{nom} as the nominal voltage measurement. Then, we deploy a parallel KO to estimate the potential prediction error E_p such that $E_p = V_{nom} - V_p$. We adopt a similar delay embedding strategy as presented in the Section 2.2 to learn the error dynamics and also use the charging current data as input. However, V_{nom} is only available during nominal operation ($\delta = 0$), and thus, once the secure estimation is activated, this potential Koopman approximation error E_1 is similarly self-learned, where E_1 is the Koopman prediction for E_p . Hence, this parallel KO for the error dynamics utilizes the predicted error data stack ζ_E (16) along with the input data stack ζ_U (7) to learn the self-learning Koopman-based error predictor.

$$\zeta_E = [E_1^T(k+1) \ \cdots \ E_1^T(k+\tilde{S})]. \quad (16)$$

The Koopman error predictor follows similar steps as (12)-(14) to estimate the approximation error E_1 , which is then added to the predicted voltage V_p to obtain the stage I corrected voltage estimation as

$$\text{Stage I correction: } \bar{V}_p = V_p + E_1. \quad (17)$$

This stage I corrected voltage estimation is then used as self-learning feedback for the Koopman voltage predictor as (18). Thus, after stage-I correction, the Koopman voltage predictor utilizes the data stack $\zeta_{\bar{V}_p}$ and ζ_U to learn the battery model and generate the self-learned voltage prediction V_p .

$$\zeta_{\bar{V}_p} = [\bar{V}_p^T(k+1) \ \cdots \ \bar{V}_p^T(k+\tilde{S})]. \quad (18)$$

The self-learned approximation error compensation E_1 while largely improves the self-learned voltage estimation, it still fails to capture the higher-order battery dynamics. Thus, we add stage II compensation using two different methods. While the first method adopts a heuristic approach based on our empirical findings, the second one adopts a data-driven approach. With this stage II correction, we obtain the final error-compensated secure voltage estimation \hat{V} using the comprehensive error compensation E_2 . In subsequent sections, we introduce the heuristic and data-driven strategies to compute stage II error compensation E_2 from stage I error compensation E_1 .

3.3 Heuristic Stage II: Higher-order dynamics correction with OCV-SOC mapping

Our goal in heuristically correcting the error compensation E_2 is to capture the higher-order dynamics in the true voltage V_{nom} based on the charging current. From physics-based battery models such as equivalent circuit or electrochemical models, we know that the battery terminal voltage has a strong relation with the battery OCV through the

current or the SOC. Therefore, we consider that higher-order dynamics in true voltage V_{nom} can be captured by tracking the higher-order characteristic changes in OCV with corresponding changes in SOC. However, to reduce dependencies on system knowledge and sensor redundancy, we consider that in addition to the available data (8)-(11), only the nominal battery capacity Q , OCV vs SOC map, and initial SOC at the onset of EV charging are known to us. Most importantly, these data are more readily accessible, and the OCV-SOC map does not vary with factors such as aging or operating conditions except for battery cell chemistry.

We first adopt the Coulomb counting method to calculate the SOC from the current I_c , capacity Q , and initial $SOC(0)$ data as $SOC(k+1) = SOC(k) + (\Delta t I_c)/Q$, where Δt is the sampling time. Next, the calculated SOC and the OCV-SOC map are utilized to track changes in OCV, and in turn, estimate the drift in true voltage V_{nom} from higher-order dynamics. Moreover, our empirical analysis shows that the error accumulation in the stage I compensated prediction varies between different regions of the SOC. This finding is also congruent with the characteristic changes in the OCV-SOC map. We further observe that the current flow direction during the charging vs discharging of the battery also impacts the error accumulation. Hence, we propose the following algebraic formula to obtain the OCV-SOC map-dependent heuristic correction based on our empirical observations as follows:

$$E_2 = h(SOC, sgn(I_c))E_1 + [1 - SOC] \Delta OCV. \quad (19)$$

Here, the function $h(SOC, sgn(I_c))$ exhibits a piece-wise constant mapping to SOC that varies with the charging direction $sgn(I_c)$, and the sign function $sgn(I_c)$ returns 1 for discharging and -1 for charging. $\Delta OCV(k) = OCV(k) - OCV(k-1)$ is the changes in OCV with charging. To learn this $h(SOC, sgn(I_c))$ function, we first leverage the OCV-SOC map to divide the SOC range into N_j regions and heuristically deduce the $h(SOC, sgn(I_c))$ mapping for each region and for both charging-discharging. In particular, we consider the $\frac{d^2 OCV}{d SOC^2} = 0$ and $\frac{d^3 OCV}{d SOC^3} = 0$ points as the regional SOC nodes to capture the changes in slope and curvature of the OCV-SOC map. Now, the self-learning Koopman-based error predictor is similarly affected by the lack of new information in the self-learning feedback. Thus, the comprehensive error compensation E_2 is used as self-learning feedback to the Koopman error predictor that utilizes the data stacks ζ_{E_2} (20) and ζ_U (7) to generate the approximation error prediction E_1 .

$$\zeta_{E_2} = [E_2^T(k+1) \quad \dots \quad E_2^T(k+\tilde{S})], \quad (20)$$

$$\zeta_{\hat{V}} = [\hat{V}^T(k+1) \quad \dots \quad \hat{V}^T(k+\tilde{S})]. \quad (21)$$

Additionally, the comprehensive error compensation E_2 is added to voltage prediction V_p to obtain secure estimation:

$$\text{Heuristic Stage II correction: } \hat{V} = V_p + E_2. \quad (22)$$

Next, the error-compensated secure voltage estimation \hat{V} is sent to the cloud-BMS as well as to the self-learning KO as feedback $\zeta_{\hat{V}}$ (21).

3.4 Data-driven Stage II: Higher-order dynamics correction with GPR

For this data-driven method, we adopt the Gaussian process regression (GPR) to directly approximate the comprehensive error compensation E_2 . GPR is a non-parametric supervised regression technique and it works based on the Gaussian process (GP) concept. Accordingly, it assumes that the probability distribution for any inputs θ over a function $G(\theta)$ exhibits a Gaussian distribution and can be described as $G(\theta) \sim GPR(M(\theta), \kappa_G(\theta_i, \theta_j))$. Here, $M(\theta)$ is the mean function and κ_G is pair-wise kernel function. Thus, GPR attempts to find the underlying structure of the data points while providing the predictions as probability distributions [36]. In addition, GPR is particularly effective in cases where the relationship between the input and output variables is unknown or complex. Hence, we choose GPR to approximate the error compensation E_2 .

We utilize the error in secure estimation without a stage II compensation to approximate the compensation E_2 with our GPR model. Hence, the target data for our GPR model is $E_2 = V_{nom} - \bar{V}_p$, where V_{nom} is the nominal module voltage measurement and \bar{V}_p is the only stage I corrected voltage prediction. Moreover, we consider self-learned approximation error compensation E_1 , stage I corrected prediction \bar{V}_p , current I_c , and calculated SOC as input to our GPR model, i.e., $\theta = [E_1^T \quad \bar{V}_p^T \quad I_c \quad SOC]^T$. We train the GPR model to learn the latent mapping from the input θ to the compensation E_2 as $E_2 = G(\theta) + \eta$, where $\eta \sim \mathcal{N}(0, \sigma_\eta^2)$ is a zero-mean Gaussian noise. We adopt the squared exponential kernel function (23) and a constant basis mean function as $M(\theta) = \beta$.

$$\kappa_G(\theta_i, \theta_j) = \sigma_G^2 \exp\left(-\frac{(\theta_i - \theta_j)^2}{2 L^2}\right). \quad (23)$$

These 4 hyperparameters $\beta, \sigma_G, L, \sigma_\eta$ are optimized with the Quasi-Newton method to learn the GPR model \mathcal{G} . Furthermore, since our empirical findings highlight the SOC-dependent error accumulation due to higher-order dynamics, we similarly consider N_j regions in the SOC range for this method. Hence, we trained separate GPR models \mathcal{G}_j for the j -th SOC region to obtain the most accurate voltage estimates. Finally, we utilize these pre-trained GPR models to estimate comprehensive error compensation E_2 as

$$E_2 = \mathcal{G}_j(\theta), \quad \theta = \begin{bmatrix} E_1^T & \bar{V}_p^T & I_c & SOC \end{bmatrix}^T. \quad (24)$$

Similarly, the comprehensive error compensation E_2 is used to generate the secure estimation as

$$\text{GPR Stage II correction: } \hat{V} = V_p + E_1 + E_2. \quad (25)$$

However, for the GPR correction, the self-learning Koopman-based voltage and error predictors are not updated, respectively, with the secure estimation \hat{V} and the comprehensive error compensation E_2 feedback. Rather, the Koopman voltage predictor continues to run with stage I correction using data matrices $\zeta_{\bar{V}_p}$ and ζ_U , and the Koopman error predictor continues to utilize data matrices ζ_E and ζ_U . The secure estimation \hat{V} is sent to cloud-BMS to ensure safe battery charging.

Algorithm 1: Generate Secure Module Voltage Estimation

Input: Time instant k , module voltage measurements V , charging current input I_c , calculated SOC , choice of corrector μ , heuristic function $h(SOC, sgn(I_c))$, pre-trained GPR models \mathcal{G}_j .

Output: Secure voltage estimation \hat{V} .

```

1 for  $k \geq 0$  do
2   if  $\delta \neq 0$  then
3      $[\hat{V}] \leftarrow \text{Secure Estimator } (\zeta_{\hat{V}}, \zeta_U)$ 
4     return Secure Estimation  $\hat{V}$  ;
5   else
6      $[V_p] \leftarrow \text{Koopman Predictor } (\zeta_V, \zeta_U)$  return Voltage Prediction  $V_p$  ;
7 function Koopman Predictor( $\zeta_{(\cdot)}, \zeta_U$ ):
8   Evaluate  $P = C_{\mathcal{L}} z$  (12); return  $P$  ;
9 function Secure Estimator( $\zeta_{\hat{V}}, \zeta_U$ ):
10  if  $\mu == \text{"Heuristic"}$  then
11     $[V_p] \leftarrow \text{Koopman Predictor } (\zeta_{\hat{V}}, \zeta_U);$ 
12     $[E_1] \leftarrow \text{Koopman Predictor } (\zeta_{E_2}, \zeta_U);$ 
13    Calculate  $E_2$  with  $h(SOC, sgn(I_c))$  using (19);
14    Evaluate  $\hat{V} = V_p + E_2$  (22);
15  else
16     $[V_p] \leftarrow \text{Koopman Predictor } (\zeta_{\bar{V}_p}, \zeta_U);$ 
17     $[E_1] \leftarrow \text{Koopman Predictor } (\zeta_E, \zeta_U);$ 
18    Calculate  $\bar{V}_p = V_p + E_1$  (17);
19    Predict  $E_2$  with  $\mathcal{G}_j$  (24);
20    Evaluate  $\hat{V} = \bar{V}_p + E_2$  (25);
21 return Secure Estimation  $\hat{V}$  ;

```

Fig. 2 illustrates the overall self-learning feedback mechanism along with the two stages of error compensation for our proposed secure estimator. Furthermore, the Algorithm 1 captures the implementation steps of the self-learning Koopman-based secure estimator.

4 Simulation Results

4.1 Data Generation with Pybamm-liionpack

We have utilized the ‘liionpack’ extension of the open-source battery simulator PyBaMM (Python Battery Mathematical Modeling) to generate our EV charging scenarios [27]. The PyBaMM-liionpack framework has emerged as a

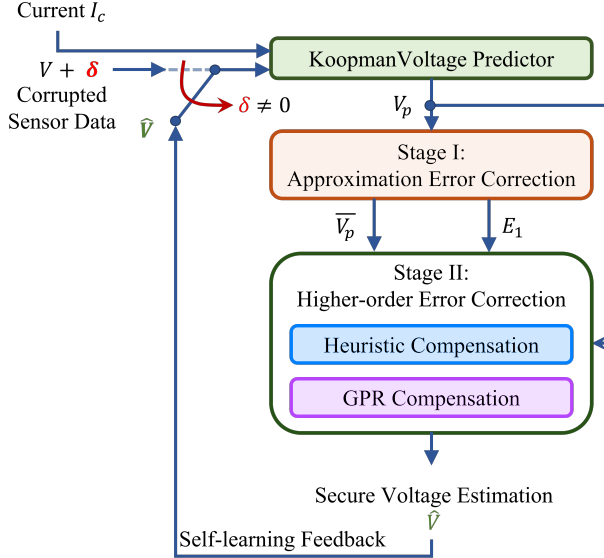


Figure 2: Block diagram showing the components of the secure estimator along with the sensor attack-triggered self-learning feedback mechanism.

reliable and powerful tool that is tailored for efficiently conducting high-fidelity battery simulations [37]. The modular architecture of the simulator supports different experiment protocols across several physics-based battery models, diverse pack configurations, and a wide range of pre-defined parameter sets for common cell chemistries. Therefore, we validate the efficacy of our proposed secure estimator with liionpack generated battery charging data. We have listed below the configurations considered during our data generation using PyBaMM.

1. **Cell Chemistry:** We have considered the commercial cylindrical battery cell LGM50 [38] to evaluate the performance of our proposed algorithm. The nominal discharge capacity of these cells is 5 Ah between the lower and upper cut-off voltages of 2.5 V and 4.2 V, respectively.
2. **Electrochemical Model:** We utilize the Single-Particle Model (SPM) in liionpack to conduct our battery experiments [39]. The SPM is an electro-chemical model that captures the internal battery dynamics and renders good accuracy while offering a computationally efficient and less complex battery model [40].
3. **Pack Configurations:** We have evaluated our secure estimator algorithm on three large-format battery packs commensurate with standard EV battery specifications [41].
 - (a) We consider a battery pack of 900 LGM50 cells and the cells are configured in 3 parallel modules with 5p60s format, i.e. 60 series branches of 5 parallel cells. The maximum voltage of the pack is 250 V, and the nominal discharge capacity is 75 Ah with a nominal energy capacity of 16 kWh.
 - (b) The second battery pack contains 2000 LGM50 cells that are arranged in 5 parallel modules with 5p80s format. The maximum voltage of the pack is 335 V, and the nominal discharge capacity is 125 Ah with a nominal energy capacity of 35 kWh.
 - (c) The third battery pack also contains 2000 LGM50 cells, however, with a different configuration. These cells are arranged in 4 parallel modules, where each module has a 5p100s format. The maximum voltage of the pack is 420 V, and the nominal discharge capacity is 100 Ah with a nominal energy capacity of 35 kWh.
4. **Charging policy & aging data generation:** For all of our experiments, we adopt the constant-current charging and discharging policy with 1C charging rate for all packs. To generate battery aging data, we repeatedly charge and discharge the battery packs between 0.3 and 0.7 SOC for 100 cycles, and we consider resting the battery for 15 minutes after each charging or discharging phase.
5. **Data Sampling:** We sample our module voltage measurement data at a 1 Hz rate, i.e., one sample per second.
6. **Generation of the OCV-SOC map:** To obtain the OCV-SOC mapping for our battery packs, we first generate the OCV-SOC map for a single-cell LGM50 battery by measuring the cell voltage at each SOC [42]. Hence, we slowly charge the single-cell battery with 0.05 A (1/100th C-rate) and measure the terminal voltage once a second to capture the OCV at the corresponding SOC. Here, the SOC is similarly calculated using the

Coulomb counting method. This cell-level OCV-SOC map is then scaled to each battery pack by multiplying with the total number of cells in that pack. Thus, we generate the measurement-based OCV-SOC map as a look-up table for our experiments.

4.2 Preliminary analysis

Determining the appropriate SOC regions is crucial to ensure reliable stage II correction using both heuristic and data-driven methods for our proposed secure estimator. Hence, we analyze the OCV-SOC map and, specifically, inspect the $\frac{d^2 OCV}{d SOC^2} = 0$ and $\frac{d^3 OCV}{d SOC^3} = 0$ points to identify the changes in the slope and curvature of the OCV-SOC map, respectively. Next, these points are used to partition the SOC range into the 14 regions utilized for our stage II correction. Fig. 3 presents the OCV-SOC curve (top), $\frac{d OCV}{d SOC}$ graph (second), $\frac{d^2 OCV}{d SOC^2}$ graph (third), and $\frac{d^3 OCV}{d SOC^3}$ graph (bottom) for this battery. In addition, the dotted line in each plot of Fig. 3 marks the 14 SOC regions, also highlighted by alternating shaded backgrounds. We have also indicated the $\frac{d^2 OCV}{d SOC^2} = 0$ corresponding boundary points with blue circles and the $\frac{d^3 OCV}{d SOC^3} = 0$ corresponding points with purple circles.

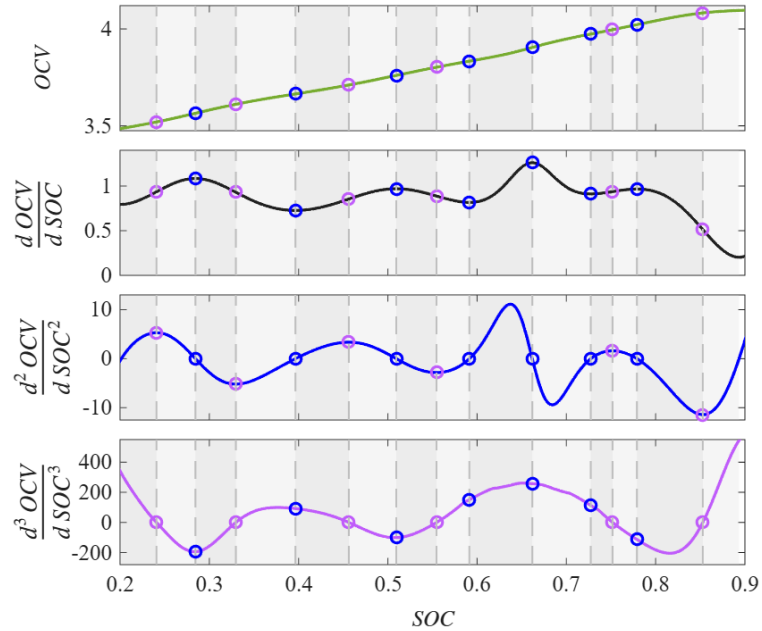


Figure 3: For the LGM50 Lithium-ion battery, the figure exhibits OCV-SOC (top), $\frac{d OCV}{d SOC}$ (second), $\frac{d^2 OCV}{d SOC^2}$ (third), and $\frac{d^3 OCV}{d SOC^3}$ (bottom) graphs.

Next, we learn the region-specific stage II corrections for both heuristic and data-driven methods to incorporate these higher-order characteristic changes of OCV into our self-learning Koopman-based secure estimator. For the heuristic method, we use a brute-force strategy to derive the constant pieces values of $h(SOC, sgn(I_c))$ in each SOC region, and Table 1 lists these values where the SOC interval $\mathcal{I}_{s,j}$ is mentioned for each region j beside the region number. Moreover, the intrinsic dynamics of the OCV-SOC mapping remains nearly unchanged among packs and single-cell battery with the same cell chemistry. Hence, we utilize the same values for $h(SOC, sgn(I_c))$ learned from cell-level analysis, while only scaling ΔOCV part in (19) for all of our battery packs. In contrast, our data-driven stage II correction fails to adapt with pack-to-pack variations or even intra-pack variations across the modules. Therefore, we train in total 12 separate sets of 14 region-specific GPR models corresponding to the 12 modules in three battery packs. Thus, the heuristic method exhibits better cell-to-pack scalability and improved robustness against variations across the modules compared to the GPR-based data-driven method.

4.3 Estimation performance assessment

Reliable, accurate, and real-time voltage estimation with improved adaptability is essential to ensure safe and optimum control of EV charging operations. Thus, we conduct an extensive Monte Carlo simulation of 1090 test runs where we evaluate the secure estimator at different battery age-levels and self-learning initiation conditions for both charging

Table 1: Piecewise-constant values of $h(SOC, sgn(I_c))$ required for heuristic correction

SOC region j	Interval $\mathcal{I}_{s,j}$	$h(SOC, 1)$ (Discharging)	$h(SOC, -1)$ (Charging)
1	[0, 0.241)	0.989	0.960
2	[0.241, 0.284)	0.853	0.948
3	[0.284, 0.330)	0.952	0.952
4	[0.330, 0.397)	0.989	0.968
5	[0.397, 0.456)	0.955	0.955
6	[0.456, 0.510)	0.946	0.945
7	[0.510, 0.555)	0.883	0.960
8	[0.555, 0.591)	0.990	0.922
9	[0.591, 0.662)	0.999	0.990
10	[0.662, 0.727)	0.963	0.978
11	[0.727, 0.752)	0.911	0.920
12	[0.752, 0.729)	0.960	0.860
13	[0.729, 0.853)	0.967	0.880
14	[0.853, 1)	0.945	0.920

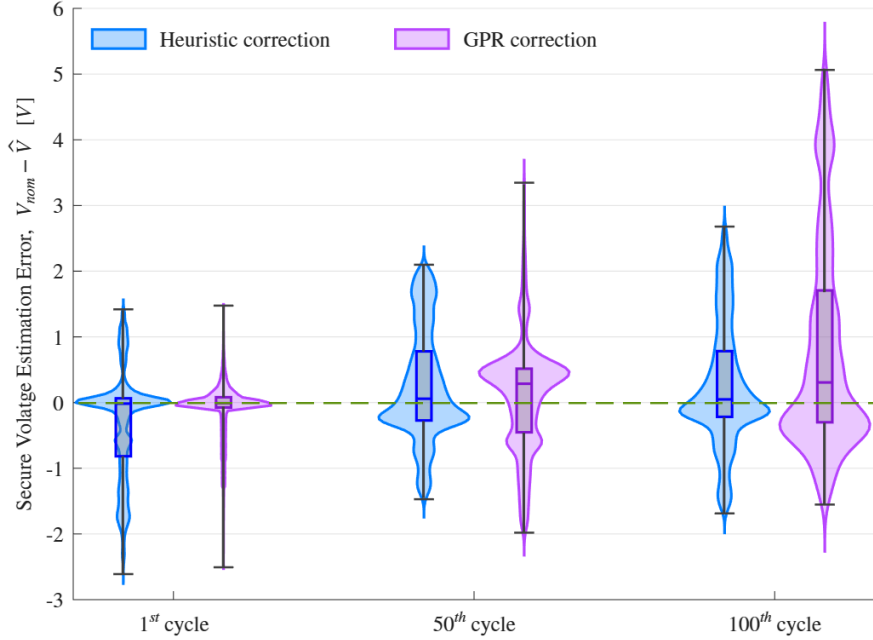


Figure 4: Plot shows the distributions of voltage estimation error for heuristic and GPR correction at three different battery age-levels.

and discharging of all packs. We use the data from these Monte Carlo runs to quantitatively analyze the algorithm's estimation accuracy, adaptability, and computational efficiency under the heuristic and GPR correction strategies. Table 2 summarizes our findings from these Monte Carlo runs at three battery age-levels- 1st, 50th, and 100th charging cycles. Fig. 4 further illustrates the distribution of estimation errors at these battery age-levels with violin plots such that the spread indicates how frequently an error value occurs. The figure also includes box plots indicating the inter-quartile range along with the median, maximum, and minimum error lines.

During testing for 1st cycle charging of battery packs, the GPR correction outperforms the heuristic correction in terms of accuracy with a lower root-mean-squared error (RMSE) of 0.4296V compared to 0.8357V RMSE for the heuristic

Table 2: Estimation performance comparison

Battery Age	Parameters	Methods	
		Heuristic	GPR
1 st cycle	RMSE [V]	0.8357	0.4296
	Maximum Overestimation [V]	2.611	2.508
	Maximum Underestimation [V]	1.419	1.489
50 th cycle	RMSE [V]	0.8671	0.8718
	Maximum Overestimation [V]	1.471	1.981
	Maximum Underestimation [V]	2.098	3.347
100 th cycle	RMSE [V]	0.9646	1.8252
	Maximum Overestimation [V]	1.687	1.552
	Maximum Underestimation [V]	2.678	5.063
Overall	Estimation Time [ms]	0.112	0.293

correction. However, the GPR correction adapts poorly to changes in battery dynamics with aging and exhibits 103% and 325% escalations in RMSEs for 50th and 100th cycle testings, respectively. In contrast, the heuristic correction demonstrates improved adaptability to battery aging with 4% and 15% increases in RMSEs for 50th and 100th cycle testings, respectively. Furthermore, Fig. 4 shows that for heuristic correction, the widest error spreads and the median errors stay close to zero for all battery age-level testings. On the other hand, while the GPR correction yields tighter error bounds for new battery testing, both error dispersions and median errors significantly shift away from zero during the 50th and 100th cycle testings, as shown in Fig. 4.

Lower values for the maximum over- and under-estimation of the voltage are crucial for efficient battery health management. Table 2 and Fig. 4 highlight that both methods exhibit an increasing trend in maximum underestimation of voltage with battery aging, while the maximum overestimation remains steady. Nevertheless, the heuristic method exhibits a maximum underestimation of 2.678V with less than 2 times rise over 100th cycle aging of the battery packs, while the GPR method exhibits 5.063V maximum underestimation with more than 3.4 times rise under similar aging conditions. Additionally, the heuristic correction achieves about 0.53 times lower RMSE and maximum underestimation than the GPR correction during the 100th cycle testing. This result illustrates the improved adaptability of the heuristic correction strategy.

In terms of resource efficiency, the GPR correction requires specific pre-trained models for each battery modules, and thus runs with a much larger computational overhead. Conversely, the heuristic correction utilizes small-data learning and limited cell-level knowledge captured by the $h(SOC, sgn(I_c))$ function, and hence runs with minimal overhead. Consequently, the heuristic correction exhibits a 2.63 times faster computational run-time compared to the GPR method and requires 0.112ms on average to estimate one sample. Nevertheless, both methods can generate estimations at a much faster rate of 3.4kHz compared to 1Hz measurement sampling rate, and thus undermine the real-time applicability of the secure estimator.

4.4 Performance evaluation under compromised sensing

In this section, we present three case studies to demonstrate the efficacy of the proposed self-learning Koopman-based secure estimator under compromised sensing, while considering different pack configurations, operating conditions, and prevalent cyberattack policies for each case study.

Case study I: Denial-of-service during discharging: In this scenario, we consider a Denial-of-service (DoS) sensor attack on the voltage measurement during discharging of the first battery pack. Consequently, the cloud-BMS ceases to receive the updated voltage measurements, rather continues to work with the last module voltage measurement received before the DoS attack. Such DoS attacks may lead to over-discharging of the battery and may also adversely impact the grid. The attack starts at 300s with a 0.819 battery SOC and continues for the next 35 minutes. This scenario is captured in Fig. 5 where the true and compromised module voltages are shown with green and red lines, respectively, in each plot. Under this DoS attack, the plots in Fig. 5 show that the Stage I correction performs poorly across all the modules. This phenomenon is expected as the Stage I corrections are not equipped to incorporate higher-order complexities of battery dynamics and continue to use the predictive slope from the last correct learning window as the basis for prediction. The plots in Fig. 5 show that both GPR and heuristic corrections estimate the module voltage with high accuracy (highlighted in the zoomed insets). Nevertheless, the GPR correction required an individually pre-

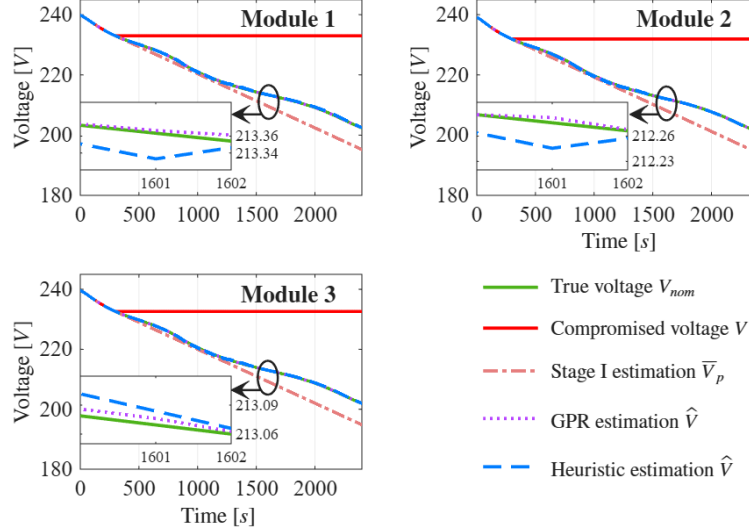


Figure 5: **DoS sensor attack:** Each plot shows the true and compromised module voltage for the battery, the voltage estimation from self-learning Koopman-based estimation with only stage I correction, with stage II GPR correction, and with stage II heuristic correction.

trained model for each module. In contrast, the same heuristic correlation with $h(SOC, \text{sgn}(I_c))$ (19) learned from a single-cell LGM50 battery is used in all modules yielded comparable accuracy. This result illustrates the improved scalability of the heuristic correction.

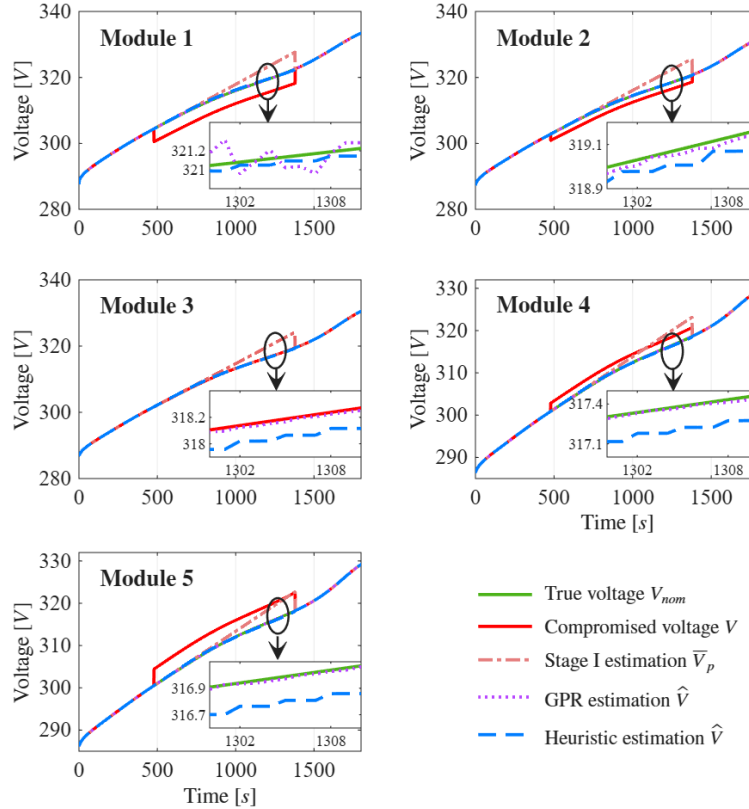


Figure 6: **Data-swap sensor attack:** Each plot shows the true and compromised module voltage for the battery, the voltage estimation from self-learning Koopman-based estimation with only stage I correction, with stage II GPR correction, and with stage II heuristic correction.

Case study II: Data-swap attack during charging: We consider a specially crafted sensor attack for this case study that swaps the module voltage data such that the ascending module voltages are rearranged to descending order [37]. Such a data-swap attack impacts the cell-balancing functionality of the cloud-BMS, leading to inefficient battery performance and impaired battery health. The attack is injected to the second battery pack for 15 minutes, starting at 480s and 0.329 battery SOC. Fig. 6 captures this scenario, and similarly, the true and compromised module voltages are shown with green and red lines, respectively, in each plot. Under this attack, the stage-I correction performance for all modules deteriorates with time as it fails to adapt to higher-order changes in the battery (shown in Fig. 6). Moreover, the plots in Fig. 6 show that both GPR and heuristic stage-II corrections provide reliable and accurate voltage estimations. The zoomed insets of the plots in Fig. 6 show that the GPR correction marginally outperforms the heuristic correction, particularly for modules 3-5. Similarly, module-specific pre-trained models are utilized for the GPR correction, while the cell-based $h(SOC, sgn(I_c))$ function (19) from the previous case study is utilized for the heuristic correction. This result further highlights the enhanced robustness towards diverse pack-configurations for the heuristic correction.

Case study III: Bias attack on aging battery: For this case study, we consider an aging battery at 100th charging cycle such that the battery capacity has degraded with aging. Consequently, under similar charging current inputs, the aged battery reaches a higher SOC level faster, leading to higher voltage measurements compared to a new battery. Fig. 7 captures this deviation in module voltage measurements with aging. The top plot of Fig. 7 shows the module voltages measured at 1st and 100th charging cycles under similar charging conditions, and the bottom plot illustrates the increment in the voltage measurements due to the battery degradation over 100 cycles.

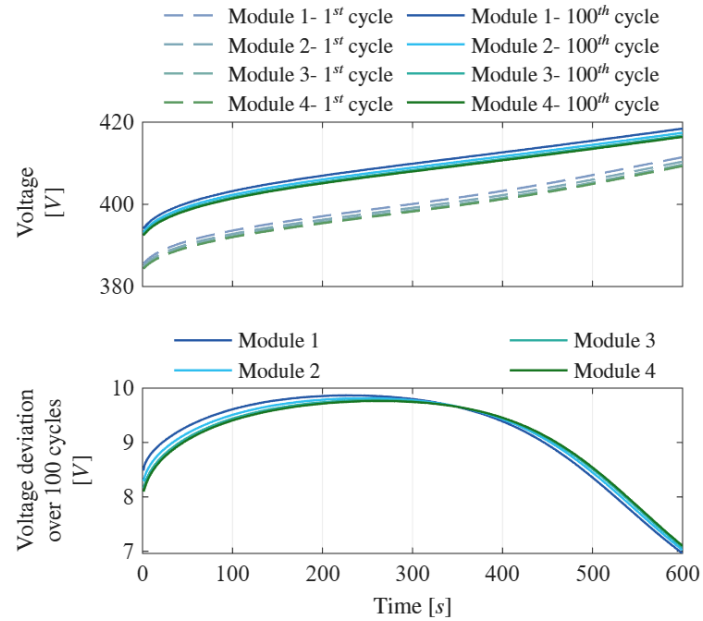


Figure 7: Battery aging: The top plot shows the module voltage measurements of the battery pack during 1st and 100th charging cycles. The bottom plot illustrates the deviation in voltage measurements for each module over these 100 cycles of battery charging.

We then consider that the adversary introduces a false-data injection (FDI) sensor attack of negative 3V bias to all module voltage measurements at 40s and continues to inject the bias attack for the remainder of the battery charging. Hence, after the first 40s of charging, the cloud-BMS receives a 3V lower voltage measurement than the true V_{nom} for all modules, which can lead to overcharging of the battery. The battery SOC at the start of the attack is 0.51. Fig. 8 captures this scenario, where each plot in Fig. 8 shows the true and compromised module voltages, respectively, with green and red lines. The stage-I correction again fails to generate reliable module voltage estimations under this FDI attack, as shown in Fig. 8. Moreover, the estimation error for the GPR correction increases with time due to the poor adaptability of the method. Conversely, the heuristic correction continues to generate highly accurate module voltage estimations for this aged battery, as highlighted in the zoomed insets of each plot in Fig. 8. Thus, this result demonstrates the improved adaptability of the heuristic correction.

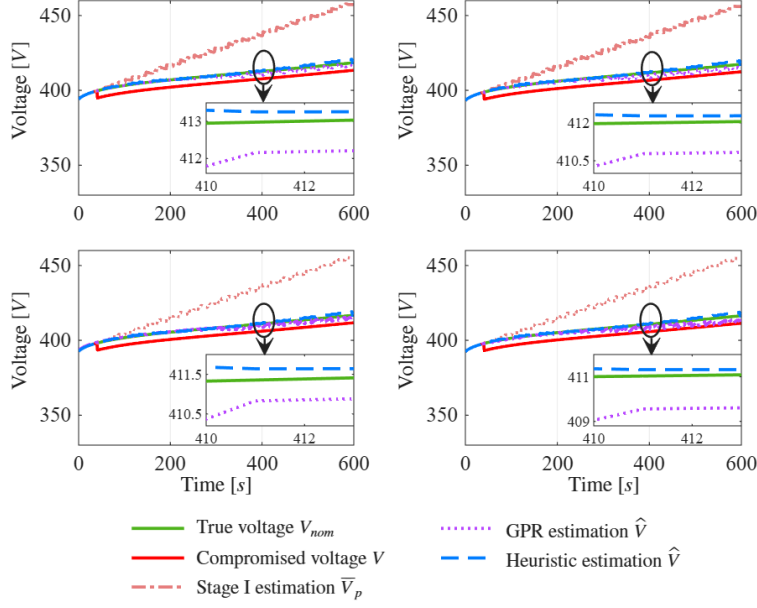


Figure 8: **FDI sensor attack on aging battery:** Each plot shows the true and compromised module voltage for the battery, the voltage estimation from self-learning Koopman-based estimation with only stage I correction, with stage II GPR correction, and with stage II heuristic correction.

5 Conclusion

In this work, we presented a Koopman-based secure voltage estimation algorithm using a two-stage error compensation integrated self-learning feedback for large-format battery packs subjected to malicious sensor attack during bi-directional charging of EVs. In stage I error correction, we estimated the potential error in voltage prediction to compensate for the error accumulation from the Koopman linear approximation. In stage II, we proposed two methods for the higher-order system dynamics corrections missed by the baseline self-learning feedback to the KO. For our first method, we propose a heuristic correction guided by our empirical findings that leverages the OCV-SOC mapping to track the higher-order dynamics in the module voltage and effectively utilizes this limited cell-level knowledge for pack-level estimation without requiring any modifications. Additionally, this heuristic correction exhibits improved adaptability to battery aging. Our second method uses a GPR-based data-driven error correction that requires minimal nominal module voltage measurements for pre-training. Our simulation case studies using high-fidelity simulation data illustrate that the proposed secure estimator generates highly accurate voltage estimation under DoS, data-swap, and FDI sensor attacks, for both new and aged battery during charging and discharging of the EVs. Such secure estimation will enable the BMS to ensure optimal, safe, and coordinated bi-directional charging of EVs while mitigating the impact of sensor cyberattacks.

References

- [1] Milad Rahmati. Edge-AI Based Multi-criteria Optimization Framework For Dynamic EV Charging With Real-time Grid Load, Traffic, And User Behavior Integration. *Computing*, 107(9):178, 2025.
- [2] Avijit Das and Di Wu. Optimal Coordination Of Electric Vehicles For Grid Services Using Deep Reinforcement Learning. In *2024 IEEE Power & Energy Society General Meeting (PESGM)*, pages 1–5. IEEE, 2024.
- [3] Ahmad Tavakoli, Sajeeb Saha, Mohammad Taufiqul Arif, Md Enamul Haque, Nishad Mendis, and Aman MT Oo. Impacts Of Grid Integration Of Solar PV And Electric Vehicle On Grid Stability, Power Quality And Energy Economics: A Review. *IET Energy Systems Integration*, 2(3):243–260, 2020.
- [4] Zuzhao Ye, Yuanqi Gao, and Nanpeng Yu. Learning To Operate An Electric Vehicle Charging Station Considering Vehicle-grid Integration. *IEEE transactions on smart grid*, 13(4):3038–3048, 2022.
- [5] Habiballah Rahimi-Eichi, Unnati Ojha, Federico Baronti, and Mo-Yuen Chow. Battery Management System: An Overview Of Its Application In The Smart Grid And Electric Vehicles. *IEEE industrial electronics magazine*, 7(2):4–16, 2013.

[6] Taesic Kim, Justin Ochoa, Tasnimun Faika, H Alan Mantooth, Jia Di, Qinghua Li, and Young Lee. An Overview Of Cyber-physical Security Of Battery Management Systems And Adoption Of Blockchain Technology. *IEEE Journal of Emerging and Selected Topics in Power Electronics*, 10(1):1270–1281, 2020.

[7] Sanchita Ghosh and Tanushree Roy. Security of cyber-physical systems under compromised switching. In 2023 *IEEE Conference on Control Technology and Applications (CCTA)*, pages 1034–1039. IEEE, 2023.

[8] Shravan Murlidharan, Varsha Ravulakole, Jyothi Karnati, and Hafiz Malik. Battery Management System: Threat Modeling, Vulnerability Analysis, And Cybersecurity Strategy. *IEEE Access*, 2025.

[9] Farshid Naseri, Zahra Kazemi, Peter Gorm Larsen, Mohammad Mehdi Arefi, and Erik Schaltz. Cyber-physical Cloud Battery Management Systems: Review Of Security Aspects. *Batteries*, 9(7):382, 2023.

[10] Samrat Acharya, Hafiz Anwar Ullah Khan, Ramesh Karri, and Yury Dvorkin. MaDEVIoT: Cyberattacks On EV Charging Can Disrupt Power Grid Operation. In 2024 *IEEE Power & Energy Society Innovative Smart Grid Technologies Conference (ISGT)*, pages 1–5. IEEE, 2024.

[11] Kenneth W Rohde. Cyber Security Of Dc Fast Charging: Potential Impacts To The Electric Grid. Technical report, Idaho National Laboratory (INL), Idaho Falls, ID (United States), 2019.

[12] Glenn Sean Morrison. Threats And Mitigation Of DDoS Cyberattacks Against The US Power Grid Via EV Charging. Master’s thesis, Wright State University, 2018.

[13] Victoria Obrien, Vittal S Rao, and Rodrigo D Trevizan. Detection Of False Data Injection Attacks In Battery Stacks Using Input Noise-aware Nonlinear State Estimation And Cumulative Sum Algorithms. *IEEE Transactions on Industry Applications*, 2023.

[14] Hyun-Jun Lee, Kyoung-Tak Kim, Joung-Hu Park, Gomanth Bere, Justin Joshua Ochoa, and Taesic Kim. Convolutional Neural Network-based False Battery Data Detection And Classification For Battery Energy Storage Systems. *IEEE Transactions on Energy Conversion*, 36(4):3108–3117, 2021.

[15] K Dhananjay Rao, Manasa Taddi, Tharun Sriramula, Dilip Kumar Baliga, Akhil Simhadri, and Parth Sarathi Panigrahy. Detection Of Cyber Attacks On Wireless Bms Of Electric Vehicles Using Long Short-term Memory Networks. In 2023 7th International Conference on Computation System and Information Technology for Sustainable Solutions (CSITSS), pages 1–6. IEEE, 2023.

[16] Mohamed ElKashlan, Mahmoud Said Elsayed, Anca Delia Jurcut, and Marianne Azer. A Machine Learning-based Intrusion Detection System For Iot Electric Vehicle Charging Stations (EVCSs). *Electronics*, 12(4):1044, 2023.

[17] Asadullah Khalid, Mohammad Khan, Alexander Stevenson, Shanzeh Batool, and Arif Sarwat. Investigation Of Cell Voltage Buffer Manipulation Attack In A Battery Management System Using Unsupervised Learning Technique. In 2021 *IEEE Design Methodologies Conference (DMC)*, pages 1–6. IEEE, 2021.

[18] Sanchita Ghosh and Tanushree Roy. Koopman operator-based detection-isolation of cyberattack: A case study on electric vehicle charging. In 2024 *American Control Conference (ACC)*, pages 2236–2241. IEEE, 2024.

[19] Licheng Wang, Engang Tian, Changsong Wang, and Shuai Liu. Secure Estimation Against Malicious Attacks For Lithium-ion Batteries Under Cloud Environments. *IEEE Transactions on Circuits and Systems I: Regular Papers*, 69(10):4237–4247, 2022.

[20] Tanushree Roy, Ashley Knichel, and Satadru Dey. An input-to-state safety approach toward safe control of a class of parabolic pdes under disturbances. *IEEE Transactions on Control Systems Technology*, 2024.

[21] S. Ghosh and Tanushree Roy. Detection And Isolation Of Battery Charging Cyberattacks Via Koopman Operator. *Applied Energy*, 401:126695, 2025.

[22] Engang Tian, Hui Chen, Changsong Wang, and Licheng Wang. Security-ensured State Of Charge Estimation Of Lithium-ion Batteries Subject To Malicious Attacks. *IEEE Transactions on Smart Grid*, 14(3):2250–2261, 2022.

[23] Shunyuan Xiao, Lei Ding, Maojiao Ye, Dong Yue, and Hui Ge. Resource-Efficient And Resilient SOC/SOH Co-Monitoring Of EV Batteries With Attack Detection. *IEEE Transactions on Smart Grid*, 2025.

[24] Shiyu Dong, Jing Liang, Yuanyuan Li, Duo Yang, Remus Teodorescu, and Jinhao Meng. Secure State Of Charge Estimation For Lithium-ion Battery: An Impulsive-Driven-Based Observer Approach. *IEEE Transactions on Transportation Electrification*, 2025.

[25] Rodrigo D Trevizan, James Obert, Valerio De Angelis, Tu A Nguyen, Vittal S Rao, and Babu R Chalamala. Cyberphysical Security Of Grid Battery Energy Storage Systems. *IEEE Access*, 10:59675–59722, 2022.

[26] S. Ghosh and Tanushree Roy. Secure Estimation Of Battery Voltage Under Sensor Attacks: A Self-Learning Koopman Approach. In 2025 *IEEE Conference on Control Technology and Applications (CCTA)*, pages 874–879, 2025.

[27] Thomas Tranter, Robert Timms, Valentin Sulzer, Ferran Planella, Gavin Wiggins, Suryanarayana Karra, Priyan-shu Agarwal, Saransh Chopra, Srikanth Allu, Paul Shearing, et al. Liionpack: A Python Package For Simulating Packs Of Batteries With PyBaMM. *Journal of Open Source Software*, 7(70), 2022.

[28] Jay Johnson, Benjamin Anderson, Brian Wright, Jimmy Quiroz, Timothy Berg, Russell Graves, Josh Daley, Kandy Phan, Micheal Kunz, Rick Pratt, et al. Cybersecurity For Electric Vehicle Charging Infrastructure. Technical report, Sandia National Lab.(SNL-NM), Albuquerque, NM (United States), 2022.

[29] Valentin Sulzer, Scott G Marquis, Robert Timms, Martin Robinson, and S Jon Chapman. Python Battery Mathematical Modelling (PyBaMM). *Journal of Open Research Software*, 9(1), 2021.

[30] Bernard O Koopman. Hamiltonian Systems And Transformation In Hilbert Space. *Proceedings of the National Academy of Sciences*, 17(5):315–318, 1931.

[31] Steven L Brunton. Notes On Koopman Operator Theory. *Universität von Washington, Department of Mechanical Engineering, Zugriff*, 30, 2019.

[32] Milan Korda and Igor Mezić. Linear Predictors For Nonlinear Dynamical Systems: Koopman Operator Meets Model Predictive Control. *Automatica*, 93:149–160, 2018.

[33] Igor Mezić. Spectral Properties Of Dynamical Systems, Model Reduction And Decompositions. *Nonlinear Dynamics*, 41:309–325, 2005.

[34] Amit Surana and Andrzej Banaszuk. Linear Observer Synthesis For Nonlinear Systems Using Koopman Operator Framework. *IFAC-PapersOnLine*, 49(18):716–723, 2016.

[35] Mahdi Taheri, Khashayar Khorasani, Nader Meskin, and Iman Shames. Data-driven Koopman Operator Based Cyber-attacks For Nonlinear Control Affine Cyber-physical Systems. In *2022 IEEE 61st Conference on Decision and Control (CDC)*, pages 6769–6775. IEEE, 2022.

[36] Kailong Liu, Xiaosong Hu, Zhongbao Wei, Yi Li, and Yan Jiang. Modified Gaussian Process Regression Models For Cyclic Capacity Prediction Of Lithium-ion Batteries. *IEEE Transactions on Transportation Electrification*, 5(4):1225–1236, 2019.

[37] S. Ghosh and Tanushree Roy. Transfer Learning Assisted XgBoost For Adaptable Cyberattack Detection In Battery Packs. *IFAC-PapersOnLine*, 59(30):917–922, 2025. 5th Conference on Modeling, Estimation and Control MECC 2025.

[38] Chang-Hui Chen, Ferran Brosa Planella, Kieran O’regan, Dominika Gastol, W Dhammad Widanage, and Emma Kendrick. Development Of Experimental Techniques For Parameterization Of Multi-scale Lithium-ion Battery Models. *Journal of The Electrochemical Society*, 167(8):080534, 2020.

[39] Sven Atlung, Keld West, and Torben Jacobsen. Dynamic Aspects Of Solid Solution Cathodes For Electrochemical Power Sources. *Journal of The Electrochemical Society*, 126(8):1311, 1979.

[40] Adrien M Bizeray, Jin-Ho Kim, Stephen R Duncan, and David A Howey. Identifiability And Parameter Estimation Of The Single Particle Lithium-ion Battery Model. *IEEE Transactions on Control Systems Technology*, 27(5):1862–1877, 2018.

[41] Luigi Sequino, Ezio Mancaruso, and Bianca Maria Vaglieco. Modeling Study Of The Battery Pack For The Electric Conversion Of A Commercial Vehicle. Technical report, SAE Technical Paper, 2021.

[42] Seongjun Lee, Jonghoon Kim, Jaemoon Lee, and Bo H Cho. State-of-charge And Capacity Estimation Of Lithium-ion Battery Using A New Open-circuit Voltage Versus State-of-charge. *Journal of power sources*, 185(2):1367–1373, 2008.